Prepared for the National Institutes of Health
National Institute of Neurological Disorders and Stroke
Division of Fundamental Neurosciences
Neural Prosthesis Program
Bethesda, MD 20892

Unassisted Standing with Functional Neuromuscular Stimulation

NIH-NINDS-N01-NS-6-2351

Progress Report #2

Period Covered:
January 1, 1997 - April 30, 1997

Principal Investigator: Ronald J. Triolo, Ph.D.
Co Principal Investigators: Robert F. Kirsch, Ph.D.
John A. Davis, Jr., M.D.

Departments of Orthopaedics and Biomedical Engineering
Case Western Reserve University
Cleveland, OH 44106-4912

Co Investigators: James J. Abbas, Ph.D.
University of Kentucky

Scott L. Delp, Ph.D.
Northwestern University

I. ABSTRACT

The long-term goal of this contract is to develop methods to provide brace-free, energy efficient standing for persons with complete thoracic level spinal cord injuries via functional neuromuscular stimulation (FNS). Our objectives are to define the fundamental requirements, develop the control strategies, and understand the factors limiting the performance of systems designed to automatically resist reasonable disturbances to balance and free the upper extremities for manipulating objects in the environment while standing. These objectives are being addressed through an organized effort consisting anatomical modeling, dynamic modeling and controller development, simulation and optimization, and experimental demonstration of new control structures. This work represents an active partnership between the investigators at Case Western Reserve University (CWRU) and collaborators at Northwestern University and the University of Kentucky. Progress during this reporting period has been made in the areas of modeling the joints and muscles of the trunk, computing system dynamics, simulating the mechanical behavior of the body in response to FNS, and adapting stimulus parameters to account for non linear recruitment properties and the time-varying effects of fatigue.

II. INTRODUCTION

Achieving independent, hands-free standing with FNS depends upon the development of an anatomical and biomechanical model of the lower extremities and torso that accurately reflects the actions of FNS on paralyzed muscle. This will be employed to construct dynamic simulations and perform optimization procedures to investigate the theoretical behavior of various FNS control systems for providing automatic postural adjustments. Predictions resulting from the modeling and simulation will drive the implementation and experimental demonstration of the postural control systems in human volunteers. Creating a new anatomical model of the trunk and integrating it into an existing three-dimensional representation of the lower extremities, adding inertial properties and developing the facility to compute dynamics, simulating and optimizing controller performance, and collecting new data to adjust the model parameters for spinal cord injury (SCI) are goals identified for the first year of the contract.

The first quarter of this year was dedicated primarily to establishing the facilities and human resources to develop the model and perform the dynamic computations required by the contract. Over the past four months, substantive progress have been made in modeling the musculoskeletal anatomy of the trunk and spine, incorporating inertial properties and computing the dynamics of human stance as a closed chain system, and creating methods to adapt for non-linear recruitment and fatigue properties of stimulated muscle. This report summarizes these results and their relationship to the overall goals of the contract.

III. PROGRESS THIS REPORTING PERIOD

Progress this reporting period was made primarily in three areas: 1) anatomical modeling of the spine and trunk, 2) biomechanical modeling and simulation, and 3) adaptive and preparatory control algorithm development.

A. Anatomical Modeling of the Spine and Trunk

We have developed a preliminary model of the trunk and integrated it with the existing model of the lower extremities using Software for Interactive Musculoskeletal Modeling (SIMM - Musculographics, Inc.). This project period was dedicated to scaling the trunk model to assure its accuracy and to defining the geometry of three key muscles (rectus abdominus, erector spinae, and quadratus lumborum). Three sets of tests were performed to assess the accuracy of the model. The first calibrates the segment lengths of the model with published data. The second evaluation compares the dimensions of individual vertebrae with those found in the literature. The third validates the moment arms computed with the model to accepted values previously reported.

1. Verification of model segment lengths: Our initial goal is to create a model that represents an able bodied subject of average stature. To accomplish this, the trunk model was scaled to maintain correct body proportions that are within one standard deviation of the average reported in several anthropometric surveys. The overall height (stature), the supersternale height (shoulder height), the iliiocristale height (pelvic height), and the trochanteric height (leg height) of the SIMM model were compared to the 15-25% (approximately -1 standard deviation), 50% (mean), and the 75-85% (approximately +1 standard deviation) percentile values obtained from four different anthropometric studies, each of which surveyed over 790 able-bodied males [1,2]. **Table I** summarizes these evaluations.

The overall stature of the SIMM model was close to the 50% percentile of the various studies (maximum deviation of 3 cm). The model height was within one standard deviation of all four studies. The supersternale height was slightly higher than the means of the four studies (maximum deviation of 4.5 cm), but within one standard deviation reported for three of the four data sets. The illiocristale height was very close to the mean reported in the Air Force and French

Table 1: Segment dimensions of the computer model compared to other studies

Model Values		Study 1 (US Army[2])	Study 2 (USAF[1])	Study 3 (French[1])	Study 4 (German[1])
Stature:	**15-25%**	169.9	170.4	168	172.3
173.4 cm	**mean**	175.5	174.5	172.1	176.5
	75-85%	181.2	178.8	176.5	180.9
Supersternale	**15-25%**	138.8	138.4	136.7	140.5
Height:	**mean**	143.7	142.3	140.6	144.1
145.1 cm	**75-85%**	148.8	146.3	144.5	147.8
Illiocristale	**15-25%**	102.9	100.1	100.9	103.4
Height:	**mean**	107.2	103.4	104.3	106.7
103.3	**75-85%**	111.6	106.9	107.6	109.9
Trochanteric	**15-25%**	88.8	88.9	88.1	88.6
Height:	**mean**	92.6	91.9	90.7	91.7
87.9 cm	**75-85%**	96.8	95.5	93.9	95.0

studies [1], but was smaller (maximum deviation of 4 cm) than the height reported in the Army [2] and German [1] studies. The trochanteric height was smaller than the values reported in all four surveys (maximum deviation of 4.5 cm). It was approximately 0.5 cm (average) outside the one standard deviation range reported by all four studies. It should be noted that although high correlations between the stature and segmental parameters such as illiocristale height have been reported, individual subjects rarely have proportional segment values. Overall, there is good agreement between the model segment lengths and those reported in the literature.

2. ***Verification of model vertebral dimensions:*** A digitized model of the spine was obtained from Viewpoint Engineering. The representation of the spine was divided into individual vertebrae and disks so that the relative motion of the bones could be described. The dimensions of the individual thoracic and lumbar vertebrae were measured and compared with published data [3-6]. These results are summarized in **Table II**. The vertebral body height (anterior and posterior) and the transverse process width were measured for each vertebra. The lumbar vertebral dimensions matched the published data very well, with deviations less than 2 mm, and all measurements close to one standard deviation range reported by both Gilad et al. and Berry et al. The thoracic vertebrae were generally larger (3-6 mm) than those in the literature. The dimensions of 3 of the 12 thoracic vertebrae fell within one standard deviation of the mean range reported by Panjabi et al. and Berry et al., while the rest of the vertebrae were greater than one standard deviation larger.

3. ***Verification of muscle moment arms:*** Three trunk muscles have been modeled: the rectus abdominus, the erector spinae, and the quadratus lumborum. The origin and insertion points of these muscles have been determined from anatomical drawings, CT/MRI images, and inspection of cadavers. Moment arms of these muscles in the upright standing position were computed and compared to published values. The erector spinae was represented as three separate segments (on each side): iliocostalis thoracis, iliocostalis lumborum and spinalis. The iliocostalis muscles originate at the angles of the 7th and 9th ribs and insert into the median and lateral sacral crests, and the medial part of the back of the iliac crest. The moment arms of the three segments in the anterior-posterior and medial-lateral direction were averaged to give the overall erector spinae moment arm. The moment arm was computed as the distance between the muscle point and the centroid of the inferior surface of a vertebra in the principal directions at that vertebral level. The rectus abdominus was represented using three segments - a medial segment, an intermediate segment, and a lateral segment. The rectus abdominus muscle originates from the fifth to the seventh costal cartilages and inserts into the pubic crest, tubercle, and symphysis. The quadratus lumborum was represented using five segments. The muscle has been described as originating from the medial part of the 12th rib and the transverse processes of the upper four lumbar vertebra and inserting into the iliac crest and iliolumbar ligament.

Table III summarizes the moment arms of the individual muscle segments in the model and the average moment arms of the three muscles in anterior-posterior and medial-lateral directions. **Table IV** shows a comparison of the average moment arms from the SIMM model at neutral position to values reported by Tracy et al. [7] and Moga et al. [8]. The average moment arms of the erector spinae were slightly higher (maximum deviation of 25% in anterior-posterior direction and 20% in medial-lateral direction) than those reported by the two studies, but very

Table II: Vertebral body dimensions (mm) and comparison of SIMM model with reported values

THORACIC	Posterior Vertebral Body Height				Transverse Process Width		Anterior Vertebral Body Height	
	Model	PANJABI et al. (1991)	BERRY et al. (1987)	SCOLES et al. (1989)	Model	PANJABI et al. (1991)	Model	BERRY et al. (1987)
T1	17.7	14.1 ± 1.9	-	16.8	91.3	75.3	17.1	-
T2	18.5	15.6 ± 3.7	16.5 + 1.2	-	70.5	69.4	17.8	17.6 + 1.2
T3	20.1	15.7 + 3.6	-	18.6	74.9	60.8	19.2	-
T4	21.4	16.2 + 2.5	-	-	73.6	56.9	20.3	-
T5	21.6	16.2 ± 4.0	-		73.6	61.1	20.5	-
T6	21.8	17.4 ± 3.2	-	19.8	73.6	61.3	20.6	-
T7	22.9	18.2 + 5.4	19.1 ± 1.8	-	73.6	60.4	20.6	18.7 ± 2.8
T8	24.2	18.7 ± 5.2	-	-	77.0	59.9	21.4	-
T9	25.7	19.3 ± 3.8	-	21.8	64.4	59.3	21.2	-
T10	30.1	20.2 ± 2.1	-	-	54.2	58.4	24.6	-
T11	28.5	21.3 + 5.6	-	-	54.2	52.2	24.5	-
T12	28.2	22.7 ± 12	24.8 ± 1.8	25.9	54.2	46.9	24.2	23.4 ± 2

LUMBAR	Posterior Vertebral Body Height			Transverse Process Width	Anterior Vertebral Body Height		
	Model	GILAD et al. (1986)	BERRY et al. (1987)	Model (no data available)	Model	PANJABI et al. (1991)	BERRY et al. (1987)
L1	26.7	27.1 ± 2.1	25.8 ± 2.1	72.4	25.2	25.4 ± 2.2	25 + 2.9
L2	25.6	28.0 ± 2.1	25.2 ± 2.2	72.4	24.9	27.2 + 2.0	27.9 + 1.9
L3	27.3	27.9 + 2.1	26 + 1.6	74.6	27.1	27.9 ± 2.1	27.4 + 1.7
L4	27.8	27.1 + 2.3	26.4 ± 1.7	74.6	28.0	27.4 ± 2.2	26.7 ± 1.5
L5	24.5	25.7 ± 2.5	23.1 ± 1.5	74.6	26.0	28.3 ± 2.1	28.7 ± 1.9

close to the one standard deviation range reported by Tracy et al. The moment arms of the rectus abdominus in neutral position matched very well compared to those reported by Tracy et al. (maximum deviation of 8% in anterior-posterior direction and 26% in medial lateral direction). The moment arms of quadratus lumborum are smaller in anterior posterior (maximum deviation of 30%) and medial lateral direction (maximum deviation of 35%) compared to the two studies. However, they lie close to the one standard deviation range reported by Tracy et al.

Table III: Anterio-posterior (AP) and medio-lateral (ML) moment arms (in mm).

a. Quadratus Lumborum

	Vertebral Attachment of Muscle Compartment										Model Average	
	T12		L1		L2		L3		L4			
	AP	ML	AP	ML	AP	ML	AP	ML	AP	ML	AP	ML
L1-L2	27.7	50.4	23.5	33.8						-	25.6	42.1
L2-L3	30.5	55.7	35.9	42.1	23.6	32.4	-	-	-		30.0	43.4
L3-L4	26.8	61.8	27.0	51.3	25.6	43.0	24.0	34.9		-	25.8	47.7
L4-L5	-		21.8	61.2	24.0	54.6	27.4	48.2	25.6	42.1	24.7	51.5

b. Rectus Abdominus

	Muscle Compartment						Model Average	
	Lateral		Intermediate		Medial			
	AP	ML	AP	ML	AP	ML	AP	ML
T12-L1	134.9	61.4	128.1	37.7	119.6	17.4	127.5	38.8
L1-L2	117.6	57.2	111.6	35.2	103.9	16.0	111.0	36.1
L2-L3	100.3	53.3	95.1	32.9	88.1	14.8	94.5	33.6
L3-L4	88.1	49.0	83.8	30.4	77.5	13.2	83.1	30.8
L4-L5	78.5	44.4	75.4	28.0	69.7	11.6	74.5	28.0
L5-S1	77.8	39.9	75.5	25.4	70.7	10.0	74.7	25.1

c. Erector Spinae

	Muscle Compartment						Model Average	
	Illiocostalis Thoracis		Illiocostalis Lumborum		Spinalis			
	ML	AP	MP	AP	ML	AP	ML	AP
T12-L1	60.6	48.9	49.6	83.1	62.5	10.9	57.5	47.6
L1-L2	64.3	45.9	53.5	77.7	65.6	12.4	61.1	45.5
L2-L3	69.6	43.2	59.1	73.0	70.6	13.6	66.4	43.2
L3-L4	68.8	40.4	58.5	68.1	69.8	14.4	65.7	40.9
L4-L5	64.4	37.4	54.5	62.7	65.1	15.7	62.9	38.6
L5-S1	51.9	34.4			52.1	16.8	52.0	25.6

Table IV: Comparison of SIMM moment arms (in mm) with published values

a. Quadratus Lumborum

	Model Average		TRACY et al. (1989)		MOGA et al. (1993)	
	AP	ML	AP	ML	AP	ML
T12-L1	23.7	44.6		-	28.0	38.0
L1-L2	23.8	43.7		-	30.5	45.5
L2-L3	26.5	44.8	35.2 ± 4.8	59.3 ± 6.6	35.0	56.0
L4-L5	25.2	48.5	34.8 ± 5.3	74.9 ± 5.0	34.0	63.0
L5-S1	24.6	51.0	34.5 ± 11.9	78.4 ± 7.4	28.5	64.0

b. Rectus Abdominus

	Model Average		TRACY et al. (1989)		MOGA et al. (1993)	
	AP	ML	AP	ML	AP	ML
T12-L1	126.7	37.6	-		141.0	45.5
L1-L2	110.4	34.9	-		135.0	45.0
L2-L3	94.4	32.1	88.6 ± 17.4	35.3 ± 8.3	122.0	45.0
L3-L4	83.2	29.9	79.6 ± 17.6	33.8 ± 9.9	110.5	42.5
L4-L5	74.4	27.3	73.9 ± 16.2	34.7 ± 8.3	104.5	39.0
L5-S1	75.1	25.1	81.3 ± 17.5	28.2 ± 8.8		-

c. Erector Spinae

	Model Average		TRACY et al. (1989)		MOGA et al. (1993)	
	AP	ML	AP	ML	AP	ML
T12-L1	57.5	47.6	-		48.5	39.2
L1-L2	64.1	45.5		-	49.5	40.0
L2-L3	66.4	43.2	57.8 ± 4.4	37.4 ± 3.5	50.5	38.2
L3-L4	65.7	40.9	57.6 ± 4.6	38.2 ± 3.2	53.5	34.0
L4-L5	62.9	38.6	60.0 ± 5.3	32.8 ± 6.0	50.5	30.5
L5-S1	52.0	25.6	61.7 ± 5.9	21.8 ± 3.9		-

4. Summary and immediate plans: The segment measurements obtained from the SIMM model matched existing anthropometric data well. The thoracic vertebrae were observed to be slightly larger than those reported in the studies by Panjabi et al., Berry et al., and Scoles et al. The lumbar vertebral dimensions matched the measurements of Gilad et al. and Berry et al. well. The overall model proportions were within one standard deviation range reported by several studies.

The moment arms calculated for the model varied slightly from the values reported in the literature. The moment arms of quadratus lumborum were about 50 percent smaller than moment arms reported by Tracy et al and Moga et al. The moment arms of the rectus abdominus matched the published data well, while the erector spinae moment arms were slightly larger (15-25%) than the values reported in the literature. Nevertheless, the preliminary moment arms in neutral position are close to the one standard deviation range of the published data.

A detailed cadaver study that will refine the model further and increase the accuracy of its representation is scheduled to begin in the last quarter of this year.

B. Biomechanical Modeling and Simulation

The mathematical representation and dynamic analysis of bipedal stance in three dimensions presents several extremely difficult technical and computational challenges. In the previous reporting period, the static, two-legged anatomical model in SIMM was successfully transferred to CWRU where it was configured to reflect bipedal standing and the reduced number of muscles likely to be activated with FNS. This three dimensional mechanical model of the lower extremities contains 12 degrees of freedom (DOF) - 2 at the ankle, 1 at the knee, 3 at the hip, bilaterally. Several major milestones related to using this model for simulation and control were accomplished during the current reporting period. These achievements include: a) integrating the segmental inertial properties and the computing of dynamic properties, b) implementing realistic constraints for foot-floor contact and the closed chain conditions imposed during bipedal stance, c) coordinating and verifying the actions of several commercially available software packages, d) predicting the postural disturbances produced by voluntary arm movements in terms of the forces and moments transmitted to the trunk at the shoulder, and e) correlating the stimulated responses of paralyzed muscle to the model output. The following section summarizes some of the details of the progress made in these areas.

1. Closed-chain model implementation: Our model of the lower extremities contains both legs, since it is not realistic to assume that the two legs of an individual with paraplegia will behave exactly alike during functional neuromuscular stimulation. Furthermore, during standing the feet typically remain stationary because of friction forces between the ground and the bottom of the feet or shoes. Under this condition, the ground and the two lower extremities form a mechanical "closed-chain", i.e., the values of the individual joint angles must add up to 360°. This closed-chain condition imposes constraints upon the independence of the joint angles. Although our bilateral model of the lower extremities contains 12 DOF, the closed-chain nature of the system reduces the actual number of independent DOF to six. The constraints can be imposed in different ways, but typically (and in our model) three are due to fixing the three-dimensional distances between the feet, and three are due to specifying the three dimensional orientation of the trunk with six DOF (three at each hip). The primary functional implication of such a closed chain model is that movements at the different joints are not independent, i.e., movement at one joint must be accompanied by movement at one or more other joints in order for the chain to remain closed.

The modeling of closed chain mechanical systems, particulary three-dimensional systems such as the lower extremity model, are complicated by several technical difficulties related to the requirement that sum of the joint angles around the chain must total 360°. First, many model simulations are based upon experimentally-measured kinematics, which will have some associated measurement error. Second, there will inevitably be some level of numerical error in

the computer simulation itself due to round-off, truncation errors, and numerical approximations (e.g., numerical derivatives of position measurements to obtain velocities and accelerations). Both types of errors will result in a sum of joint angles around the chain that is not exactly 360°. In the open chain models that have typically been used to model standing in the past, the effects of these errors will be small. However, in our more realistic closed chain model, such errors can lead to significant complications. Specifically, a typical simulation is to determine the muscle forces required to produce a certain set of measured kinematics (i.e., perform inverse dynamics). However, in the presence of kinematic errors (either measurement-related or numerical) for a closed chain, the computation of muscle forces will be dominated primarily by the attempt to close the chain. Unrealistically large and completely fictitious forces can be required to close the chain under these conditions. Such problems have led to very limited success with closed chain models in the past. Typically, simulation time is limited to a fraction of a second because such numerical errors accumulate rapidly.

We have addressed these problems in two ways. First, we have implemented a "stabilization" algorithm which distributes the errors around the chain rather than allowing them to accumulate at one location. The errors themselves are usually quite small and this redistribution has little effect on the "true" solution while significantly reducing the artifact due to forcing the chain to close. The magnitude of the remaining artifact has been further reduced by allowing some small amount of movement at the feet, rather than fixing them rigidly to the ground. This simple modification also has little impact on the "true" solution, while largely eliminating the artifact introduced into the model simulations.

Thus, we have successfully implemented a three-dimensional, closed-chain model of the lower extremities which is much more realistic than the one-legged, two-dimensional (sagittal plane) models that have been widely used in previous simulations of standing. Furthermore, we have developed methods to minimize the technical difficulties associated with this approach to acceptable levels.

2. Contact mechanics between feet and ground: As previously stated, the mathematical description of the contact mechanics between the feet and the ground have been modified to more realistically describe the actual conditions. Many models assume that the feet are fixed rigidly to the ground. Although this is approximately true during quiet standing, this assumption has two potential distorting effects. First, preventing any movement of the feet can lead to numerical difficulties in performing closed-chain simulations. Second, pinning the feet to the ground can lead to unrealistic distribution of muscle forces since this foot constraint ignores the fact that the feet will move if the friction forces between the feet and ground are exceeded. Although some movement of the feet was allowed initially as a technical solution to these problems, there are also physiological reasons for permitting such motions. The compliance of the soles of the feet and shoes, and perhaps in the ankle and in the joints of the feet, are obvious mechanisms mediating these small movements. Thus, incorporating realistic contact mechanics between the feet and ground is essential for obtaining an accurate description of the dynamics of standing posture and balance.

We have therefore replaced the static solution of fixing the feet rigidly to the floor with a dynamic constraint where the feet are fixed if the two dimensional shear forces at the foot floor interface are less than the frictional forces. However, movement is allowed if the friction forces are exceeded. This adds four additional DOF (two for each foot) to the overall model.

3. Addition of dynamic properties: One of the primary functions of the lower extremity musculature during standing is to maintain an upright posture against gravity. Furthermore, muscles must accelerate the mass of the body segments in order to make adjustments in posture, and, conversely, external force perturbations must accelerate the body segment masses in order to produce postural disturbances. Finally, muscle contractile properties are not instantaneous, so changes in muscle activation take a finite length of time to generate force. All of these dynamic properties are essential to a realistic model of the lower extremities. Thus, the second major modification of the previously existing lower extremity model was the addition of dynamic properties due to the mass and inertial properties of the various body segments and due to the contractile properties of muscle.

Values for the mass and inertial properties of the different body segments (foot, shank, thigh, and lumped head-arms-trunk) were obtained from the literature [9]. The dynamic equations of motion (i.e., the relationship between joint moments produced by muscle contraction to the resulting movement) for our 12 DOF lower extremity model were numerically implemented using a commercial dynamics software package (SD/Fast, Symbolic Dynamics, Inc.). The software routines generated by this package were then integrated into the kinematic model of the lower extremities.

Muscle contractile dynamics have initially been described mathematically using a Hill type muscle model included in the Dynamics Pipeline software from Musculographics, Inc. This model includes the length-tension and force velocity relationships for each muscle. This routine also computes estimates of energy consumption, which will be minimized in subsequent optimization procedures.

4. Postural disturbances due to upper extremity movements: Controllers designed to maintain standing posture and balance need to correct for a wide variety of internal and external disturbances. An important class of such perturbations can arise from either the volitional use of the upper extremities, or from sudden unexpected changes in the load carried by the hands. Our approach to designing controllers that allow for release and use of the upper extremities involves treating these internal disturbances as external inputs to the system by a) calculating the forces and moments produced at the shoulder during these stereotypical upper extremity activities, and b) replaying these records to the simulated control system and monitoring performance.

A computer program was developed to model the upper extremity in order to predict the forces and moments generated about the shoulder for functional arm movements. For this purpose, the upper extremity was represented as two rigid segments: the upper arm, and the lower arm (consisting of both the forearm and the hand). The connection between the two arm segments was assumed to be a hinge joint, and the shoulder was modeled as a gimbal joint to allow rotation about three axes. SD/Fast was used to numerically implement this model of the upper extremity and to solve the inverse dynamics of arm movements.

The mass, center of mass location (relative to the joints), and inertia matrices were specified for each segment as inputs into the equations of motion functions generated by SD/Fast. The default values currently in use are the averages given by McConville et al. [10], but the inertia matrices will be customized for each individual test subject when experimental data is collected to verify the program.

The program is currently configured to model the right arm, and the global reference frame is located with the shoulder joint as its origin. The x-axis points anteriorly, the y-axis points upward (opposite the direction of gravity), and the z-axis points laterally. The local

reference frames for the two arm segments align with the global reference frame when the arm is in the anatomical position, parallel to the body with the palm of the hand facing forward. The output of the system is always expressed in terms of these global coordinates. Solving the inverse dynamics equations requires four joint angles at each instant of time. Three Euler angle values are necessary to describe the position of the shoulder joint relative to the body, and the fourth value is the angle between the upper arm and the forearm. The program reads in these values from a text file, computes the current angular velocity, and passes the state information to the SD/Fast function which calculates the reaction forces and moments for that state. This information is written to another text file.

No experimental data has been recorded yet for functional arm movements, but simple output from the program is provided to demonstrate the results from three simulated arm movements. All three arm movements take place over a one second time period and were synthesized from sigmoidal angular trajectories. The first arm movement simulated was pure abduction of the arm at the shoulder, starting from anatomical position and ending perpendicular to the body in the coronal plane. The elbow joint was held in full extension throughout the movement. The second simulated movement consisted of simultaneous abduction of the shoulder and flexion of the elbow, so that the final position of the upper arm was the same as in the first movement, but with the lower arm perpendicular to the upper arm in a transverse plane (with the palm of the hand facing toward the midsagittal plane). The third movement also resulted in the same final posture, but the abduction of the shoulder and the flexion of the elbow occurred sequentially, rather than simultaneously.

The predicted forces in the x-direction were small for all three movements, especially for pure abduction, since there are no Coriolis forces resulting from the lower arm. The forces generated in the y-direction, as shown in **Figure 1**, were far greater than the forces in the x- or z-directions since this is the direction in which gravity is acting. The body sustains a constant load of approximately 40N when the arm is not moving, and this force increases when the arm is accelerated upward. It remains unchanged during the second half of the third arm movement because the height of the forearm does not vary as the elbow flexes. The z axis forces resulted primarily from centrifugal force (they are highly dependent on abduction angular velocity) and were substantially larger than those acting along the x-axis.

The moments estimated about the x axis are depicted in **Figure 2**. The moments about the y- and z-axes were significantly smaller since the primary component of all simulated movements was abduction. The z-axis moments prevent upper arm from internally rotating due to the weight of the forearm, and the y axis moments are due only to the dynamics of the arm movement, primarily the flexion of the elbow, and disappear when the arm is held in a static posture. It is interesting to note that the moment in the x-direction generated by the third arm movement peaks at the same value as the first maneuver, and then settles to the value produced by the second movement as the same final position is achieved.

These simulations demonstrate how the dynamics of arm movements can affect the forces and moments that are generated at the shoulder. Variations in speed, position, and load can dramatically affect the magnitude of resulting disturbances. We plan to study what types of disturbances will occur due to unexpected changes in load and the arm movements that result from these changes, and to validate these predictions with experimental data.

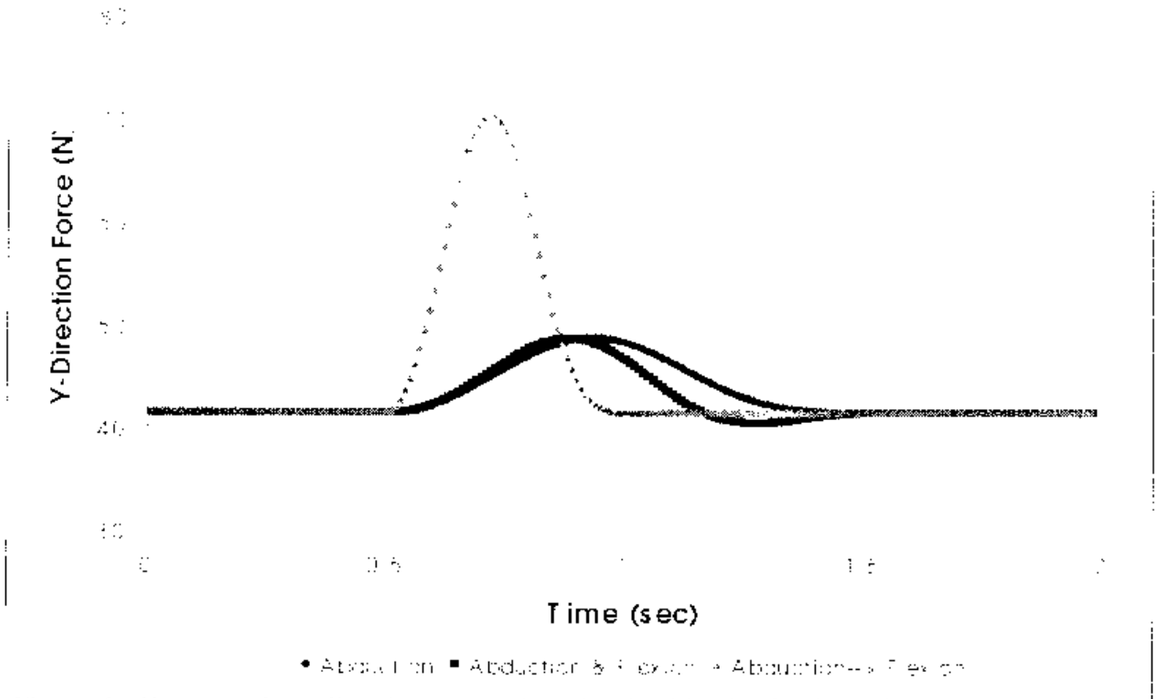

Figure 1: Forces in the y-direction (upward) at the shoulder for the three simulated arm motions

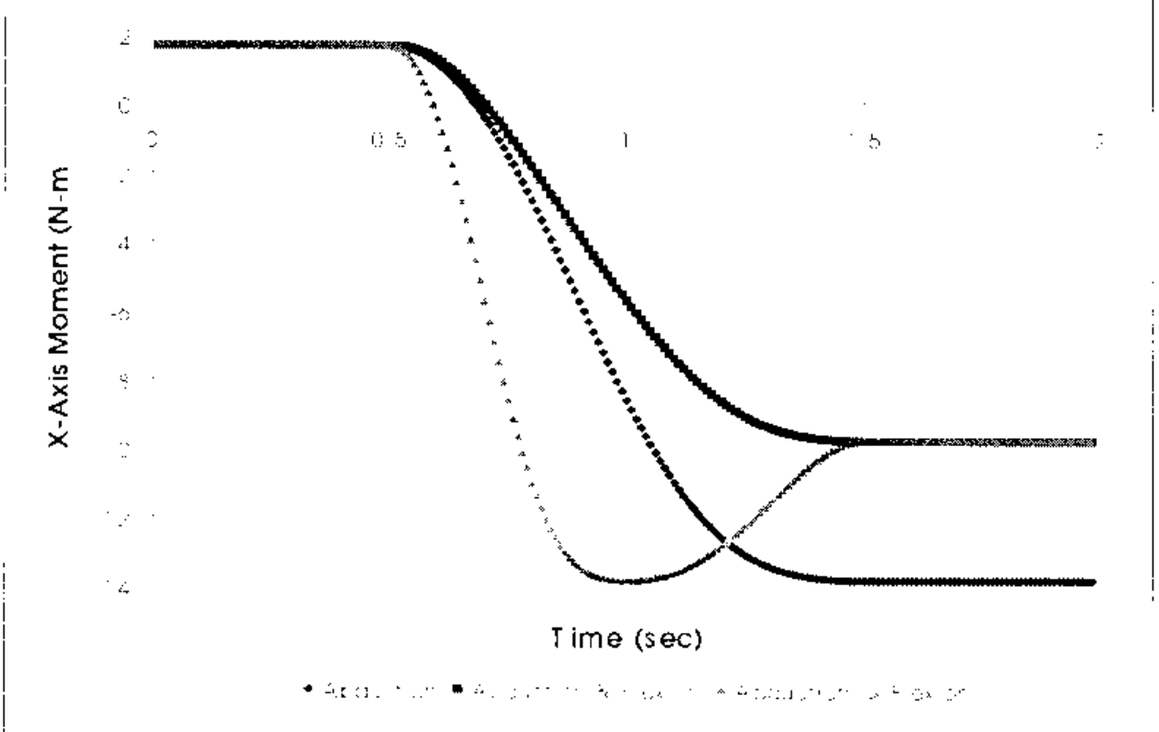

Figure 2: Moment about the x-axis at the shoulder for the three simulated arm maneuvers

5. Modeling the effects of FNS on paralyzed muscle: The anatomical model of the lower extremities currently in use is based on the properties of intact, healthy muscle from an able bodied individual. Many model parameters are likely to change after long-term spinal cord injury. Similarly, FNS may not truly activate all the fibers of interest. A goal for upcoming reporting periods is to modify the model to more accurately reflect the action of FNS on paralyzed muscle. To date, no human testing has been performed toward this end. However, data collected for other studies in our laboratory were re-analyzed to determine whether adjusting the model parameters based on assumptions about the nature of the physiological changes associated with SCI would yield reasonable results.

Initial results from analyses which compared isokinetic (45°/sec) knee extension moments produced by electrical stimulation in persons with SCI to those predicted by SIMM are encouraging. Specific model parameters such as percent muscle activation, maximum muscle force, optimal fiber length, and tendon slack length were adjusted to achieve a gross fit of the SIMM output to the SCI data. The data are preliminary, but they provide insight into the effect of altering the model to more accurately predict joint moments obtained by electrically stimulating paralyzed muscle. Typical results for the vastus lateralis (VL) muscle of one volunteer with SCI (Subject EB) are presented in **Figure 3**. In this case a reasonable match, as determined by visual inspection, was obtained by altering the optimal fiber length from 8.4cm to 10.5cm based on the assumption that prolonged periods in the sitting position may cause a stretching of the quadriceps muscles.

This type of retrospective analysis will continue on the knee and hip joint data collected during other experiments in our laboratory. The efforts will be directed toward developing an algorithm which optimizes the muscle model parameters to fit the real data based on an objective error criteria. Finally, a set of human experiments will be designed to isolate and directly measure these parameters with FNS in volunteers with spinal cord injuries.

6. Summary and immediate plans: In the current reporting period, we have largely completed the development of a 12 DOF, closed-chain dynamic model of both lower extremities, using parameters based upon able-bodied subjects. In the next period, we will begin to use this model to develop control systems for FNS-based unassisted standing. We will focus on implementing several of the controllers originally proposed, and on applying optimization techniques to identify optimal controller parameters. Controllers will be implemented initially by modifying muscle activation levels on a sample-by-sample basis depending upon the mechanical states of the model. Over the next two reporting periods this direct use of the internal muscle states will be replaced by more realistic models of actual sensors. Our approach to optimization is unchanged from the original proposal, and appropriate optimization software has been identified (Matlab Optimization Toolbox, The MathWorks, Inc.). Because of their importance to our overall approach, initial work on controller implementation and the integration of optimization will be performed using the existing able bodied model. Early in the second contract year we plan to begin to adapt the model to better reflect the physiology of spinal cord injury and the actions of FNS. Mathematical descriptions of the electrical recruitment properties of stimulated muscle and improved estimates of joint passive properties based on experimental data will be added or incorporated into the model. The predicted disturbances caused by volitional upper extremity movements will also be verified experimentally.

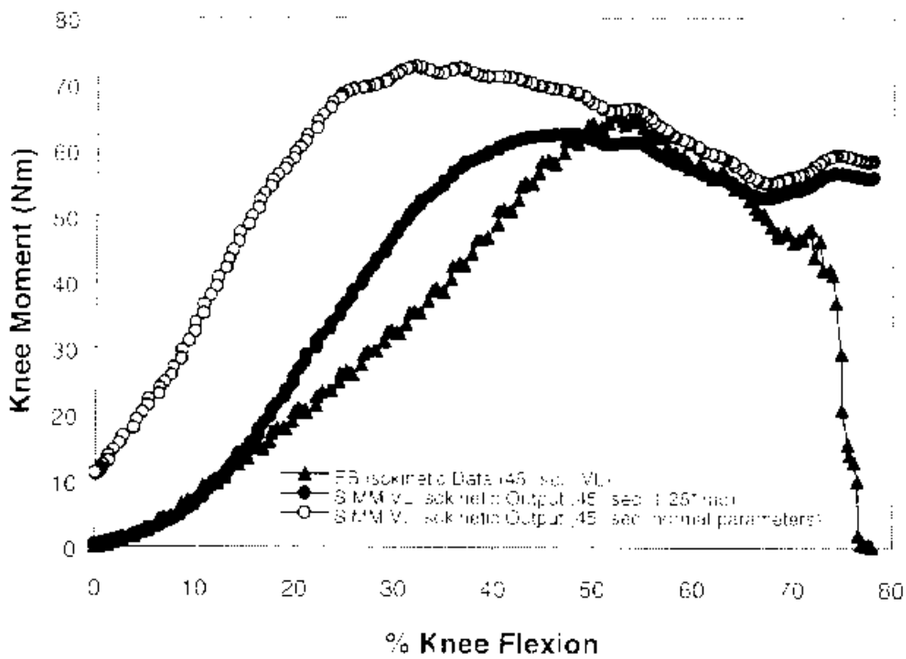

Figure 3: Isokinetic (45 /sec) knee extension moment vs. percent knee flexion as generated from the vastus lateralis (VL) of the able-bodied SIMM model (-○-), from electrical stimulation via intramuscular electrodes in an individual with a spinal cord injury (-▲-), and from a model adjusted for spinal cord injury by increasing the optimal fiber length by 25% (-●-). The SCI data were obtained from experiments performed with an instrumented CYBEX II dynamometer with the subject (EB) in a sitting position. Stimulation pulses were 60μsec in duration and 20mA in amplitude at a frequency of 20Hz. The optimal fiber length was adjusted arbitrarily in this case based on the assumption that long-term paralysis and sitting in the wheelchair for extended periods of time would increase the resting length of the muscle fibers in subject EB.

C. Adaptive and Preparatory Control Algorithm Development

Two important elements of our approach to the goal of prolonged, unassisted standing are command driven changes in posture in preparation for anticipated disturbances, and adaptation to fatigue. The former requires linearization of the recruitment properties of the stimulated muscle to simplify the user command interface. The latter involves a feedforward component to maintain adequate muscle output as the recruitment properties change. By the end of the first contract year, we plan to begin the experiments designed to characterize open loop standing, evaluate an automatic posture shifting paradigm, and implement user specified preparatory changes in posture. In this contract period, our efforts have been focused on characterizing a position sensing system that will be used for controller implementation and experimental evaluation at the University of Kentucky. The kinematic tracking system to be used at CWRU

for similar purposes has already been calibrated. We have also begun to simulate and evaluate an adaptive control system to account for nonlinear recruitment properties and changes in muscle properties due to fatigue. In the second year of the contract, we plan to have completed the development and evaluation in computer simulation of the adaptive feedforward control component so that its performance can be assessed experimentally.

I. Error characterization and correction in the kinematic tracking system: The Flock of Birds kinematic tracking system will be used in the experiments for control system implementation as well as for control system performance assessment to be performed at the University of Kentucky. This tracking system consists of a transmitter that generates an electromagnetic field and a set of four receivers that can be mounted on body segments. Each receiver can provide real time measurements of its position and orientation with respect to the transmitter. In this contract period, we have characterized the errors in position and angle measurements from the system and we have developed a method for correcting errors in the position, which were found to be unacceptable.

Four sensors were placed in each of 64 different locations to define a calibration volume of 61x72x78 cm (4 horizontal planes of 16 locations per plane). **Figure 4** shows that the x-y measurements provided by the sensors result in errors. The maximum error in distance across

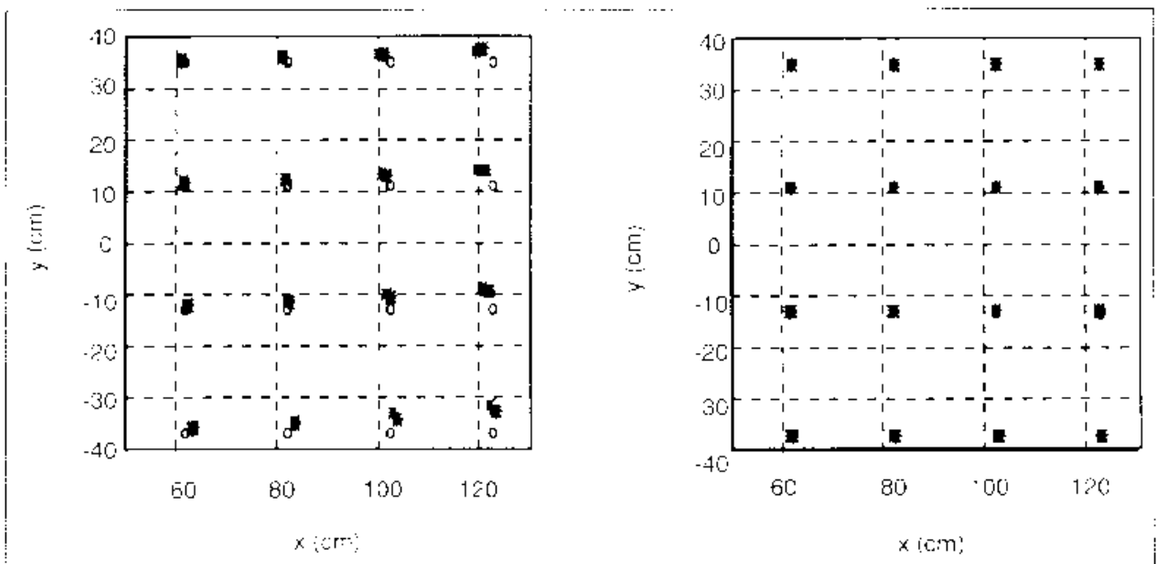

Figure 4: Position data from the Flock of Birds sensors before error compensation (left) and after compensation (right). Data were collected at 64 different locations (4 horizontal planes containing 16 measurement points) throughout the calibration volume (61x72x78 cm). The plot on the left shows the projections onto the x-y plane (horizontal plane) of the actual sensor locations (o) and the measurements from the sensors (*). The maximum error across the calibration volume was 6.52 cm, with an RMS value across the volume of 3.13 cm. The plot on the right shows the projections onto the x-y plane (horizontal plane) of the actual sensor locations (o) and the measurements from the sensors (*) after signal processing using the error correction routine described in the text. After processing, the maximum error across the calibration volume was 0.60 cm, with an RMS value across the volume of 0.22 cm. This level of accuracy should be suitable for the implementation and evaluation of the standing system.

the volume was found to be 0.52 cm. An error correction scheme was developed in which the error values were fit to polynomial functions of the distance measurement provided by the sensor. **Figure 4** also presents the 'corrected' measurements using a model that resulted in a 91% reduction in error (maximum error of 0.6 cm). Additional data (not shown) demonstrate that the measurements provided by the sensors were consistent (low 'random' noise when sensor is in a fixed location), were repeatable (measurements taken on several different days resulted in similar errors), and were independent of individual sensor characteristics (different sensors resulted in similar errors when placed in the same location).

A calibration device was constructed to allow for accurate and repeatable placement of the sensors at several different orientations. **Figure 5** shows a sketch of the device and presents results that demonstrate very small errors in angle measurements that depend on both the orientation of the sensor and the distance of the calibration device from the transmitter.

These results indicate that Flock of Birds kinematic tracking system (with the error correction described) will most likely be suitable for implementing and evaluating the standing control system. Future work will focus on characterizing the dynamic response of the system and on characterizing the angle dependence of the position error.

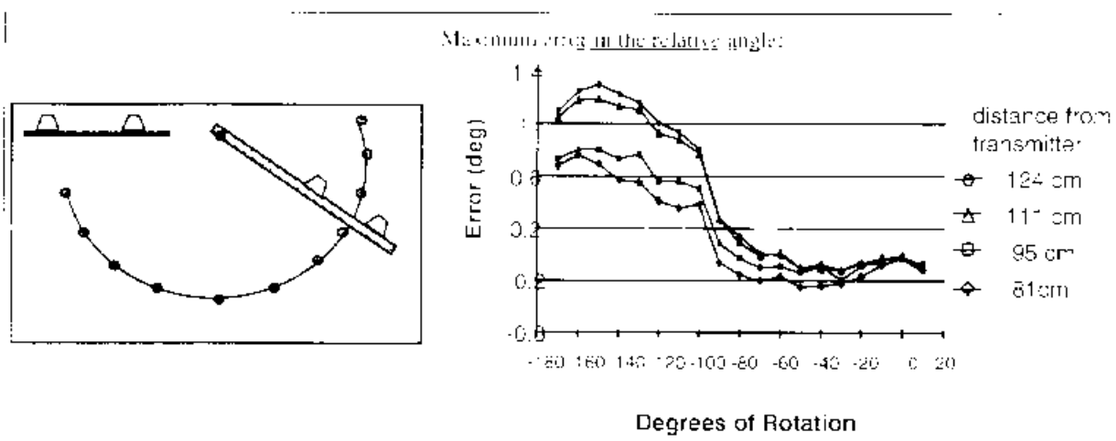

Figure 5: Angle data from the Flock of Birds sensors. The diagram on the left depicts the apparatus that was built to calibrate the angle measurements. It is a plexiglass plate with two arms attached to it, each with mounting slots for the sensors. One arm is free to rotate about one end while stops placed at increments of 10 degrees allow accurate and repeatable orientation of two sensors with respect to another two sensors. The plot on the right presents data from four calibration sessions with the apparatus placed at different distances from the transmitter. These data indicate that the errors in the angle measurements provided by the sensor system are less than 1 degree when the measurements are taken within 95 cm of the transmitter. This level of accuracy should be suitable for the implementation and evaluation of the standing system.

2. Design and development of the adaptive feedforward control system: An adaptive control system was implemented (in the Matlab environment) and the initial stage of the evaluation has been completed using computer simulated models. This stage of the evaluation has focused on a) characterizing the ability of the adaptive mapping scheme to account for nonlinearities in muscle recruitment properties and b) characterizing the ability of the adaptive mapping scheme to account for changes in the nonlinear muscle recruitment properties due to

fatigue. The model used for this initial stage of evaluation included a nonlinear recruitment curve and several variations on a model of fatigue which would result in changes in the recruitment curve over time. Therefore, the input to the controller was '%command' from the user and the output was isometric muscle torque from a single muscle. The objective of the controller in these simulations was to achieve and maintain a linear input/output characteristic as viewed by the user and to utilize the entire command range to regulate muscle torque over the range of 0-25 Nm.

Figure 6 shows the results of a simulation run that demonstrates how the adaptive mapping can account for nonlinear recruitment properties and utilize the entire command range. A technique such as this should simplify the command-control interface and allow the user to more easily specify the desired level of co-activation in preparation for a particular activity. Maintaining these linear user input/output characteristics in the presence of fatigue will be important for continuous operation for extended periods of time. **Figure 7** and **Figure 8** show the results from simulations that demonstrate how the mapping scheme is adjusted on-line to account for muscle fatigue or complicated recruitment nonlinearities. The simulations shown in **Figure 7** utilized a model of fatigue consisting of a simultaneous shift to the right of the recruitment curve, decrease in muscle gain, and drop in recruitment curve slope. All these phenomena have been observed at various times with electrically-induced fatigue. The algorithm adequately maintains the linear input/output properties. The multiple nonlinearities represented in **Figure 8** are commonly observed when paralyzed muscles are activated with FNS as large and spatially distinct nerve branches are excited with increasing stimulation. These simulations also utilized a model of fatigue consisting of only a drop in muscle gain, and again demonstrate the ability of the algorithm to account for recruitment nonlinearities in the presence of fatigue.

These results indicate that the adaptive mapping scheme can address the two primary issues for which is was designed: nonlinear recruitment and muscle fatigue. Future work will focus on further characterization and development of the adaptive component. This work will investigate the effects of other musculoskeletal nonlinearities, dynamics and hysteresis using models implemented in SIMM/SDFAST.

*3. **Summary and immediate plans:*** The primary focus of the next contract period will be to complete the setup of the laboratory hardware and software required for the experimental characterization of the open-loop control system using the posture shifting paradigm and to begin these experiments. This work will include: completion of the control system software development (including joystick interface and stimulator interface software), construction of an instrumented standing frame that can be used to provide support for the subjects when required and measurements of the support forces exerted. A secondary effort will be the continuation of the evaluation of the adaptive control system in computer simulations. This work will include incorporation of the adaptive control system algorithm into the SIMM/SDFAST environment.

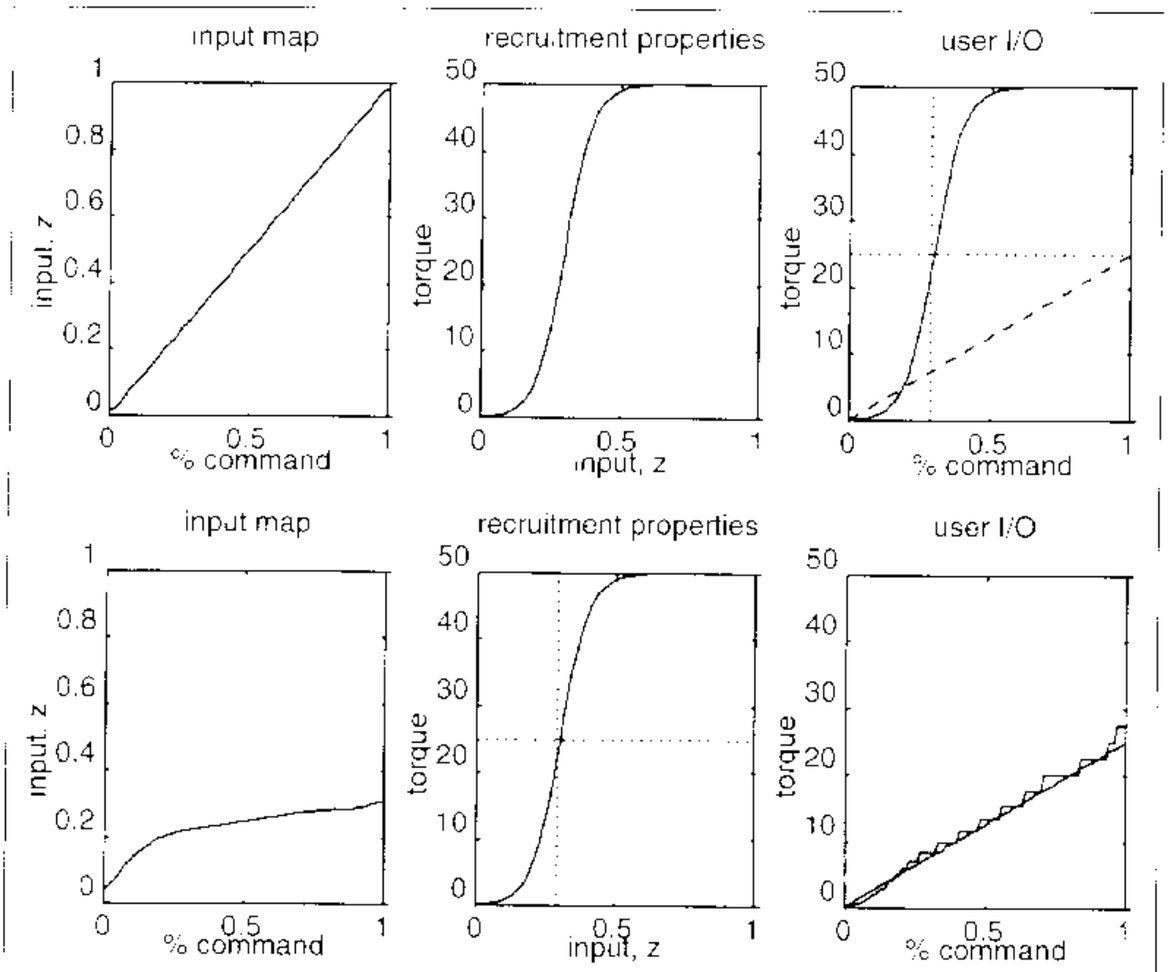

Figure 6: Simulation results demonstrating how the adaptive mapping scheme can linearize the input/output properties of stimulated muscle. In these simulations, the mapping function (left panel) was cascaded with the recruitment properties (center panel) to result in the overall input/output as seen by the user (right panel). The objective of the algorithm was to linearize the input/output properties as seen by the user and to utilize the full range of command to regulate outputs over the range of 0-25 Nm. The top three panels show the mapping function, recruitment curve and their cascade before adaptation. Note that the user input/output properties are nonlinear and that only approximately 30% of the command range is used to regulate the output. The bottom three panels show the mapping function, recruitment curve and their cascade after 20 epochs of adaptation. Note that the nonlinear mapping function (bottom left panel) results in linear user input/output properties and that the full range of command is used to regulate outputs over the range of 0-25 Nm.

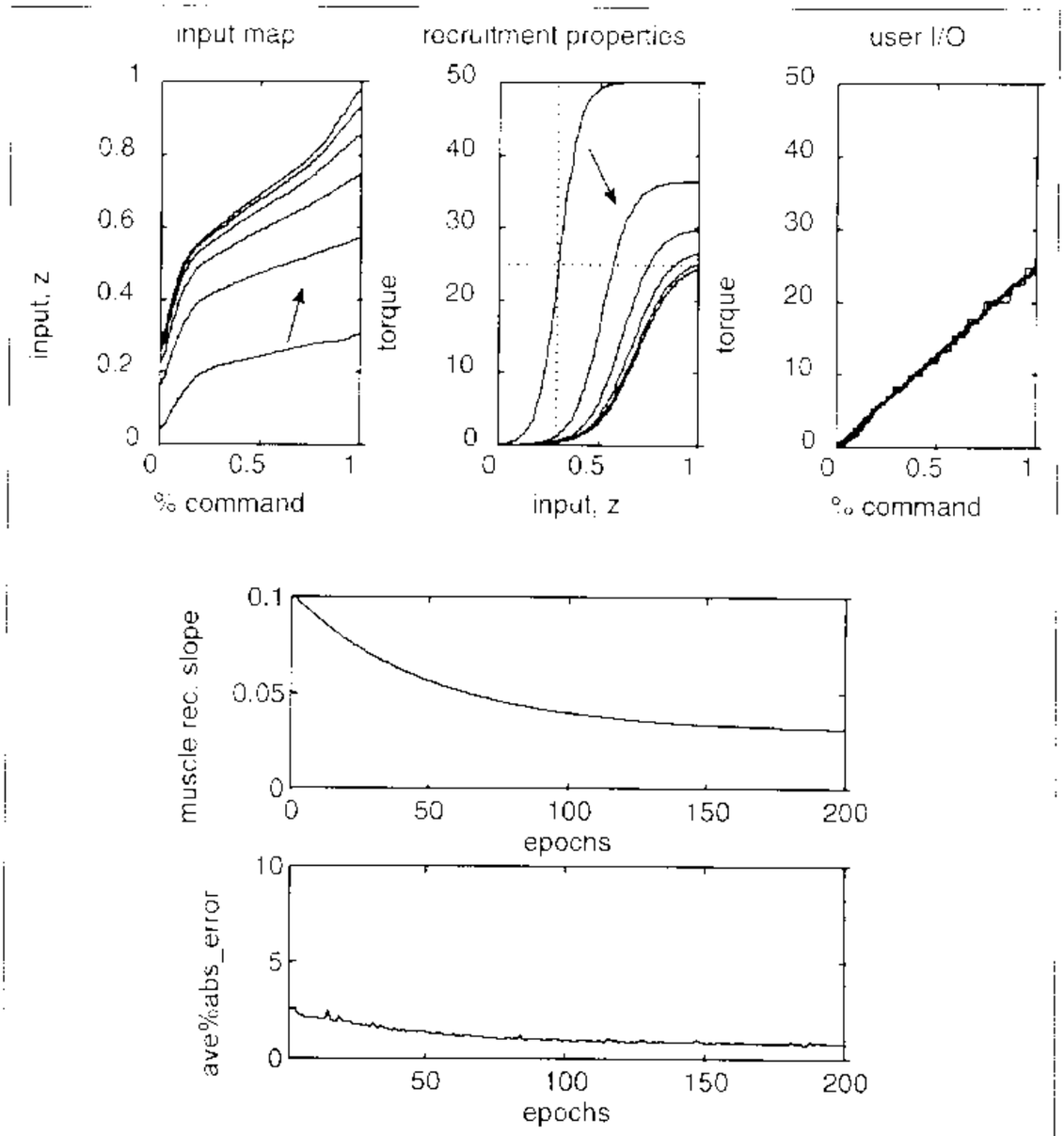

Figure 7: Simulation results demonstrating how the adaptive mapping scheme can maintain linear input/output properties as seen by the user as the muscle fatigues. The top row of plots shows the mapping function (left panel), recruitment properties (center panel) overall input/output as seen by the user (right panel). Each plot includes five lines that are 'snapshots' of the system as the trial proceeds. Note that changes in the recruitment properties result in changes in the mapping function, but that the linear input/output properties are maintained throughout the trial. In these simulations, the model of muscle fatigue includes a simultaneous drop in muscle gain, drop in recruitment curve slope and shift to the right of the recruitment curve. The plot in the second row shows the change in the midpoint of the recruitment curve as the trial progresses. The bottom plot indicates that the average of the percent of the absolute value of the error is maintained at about 3% throughout the trial.

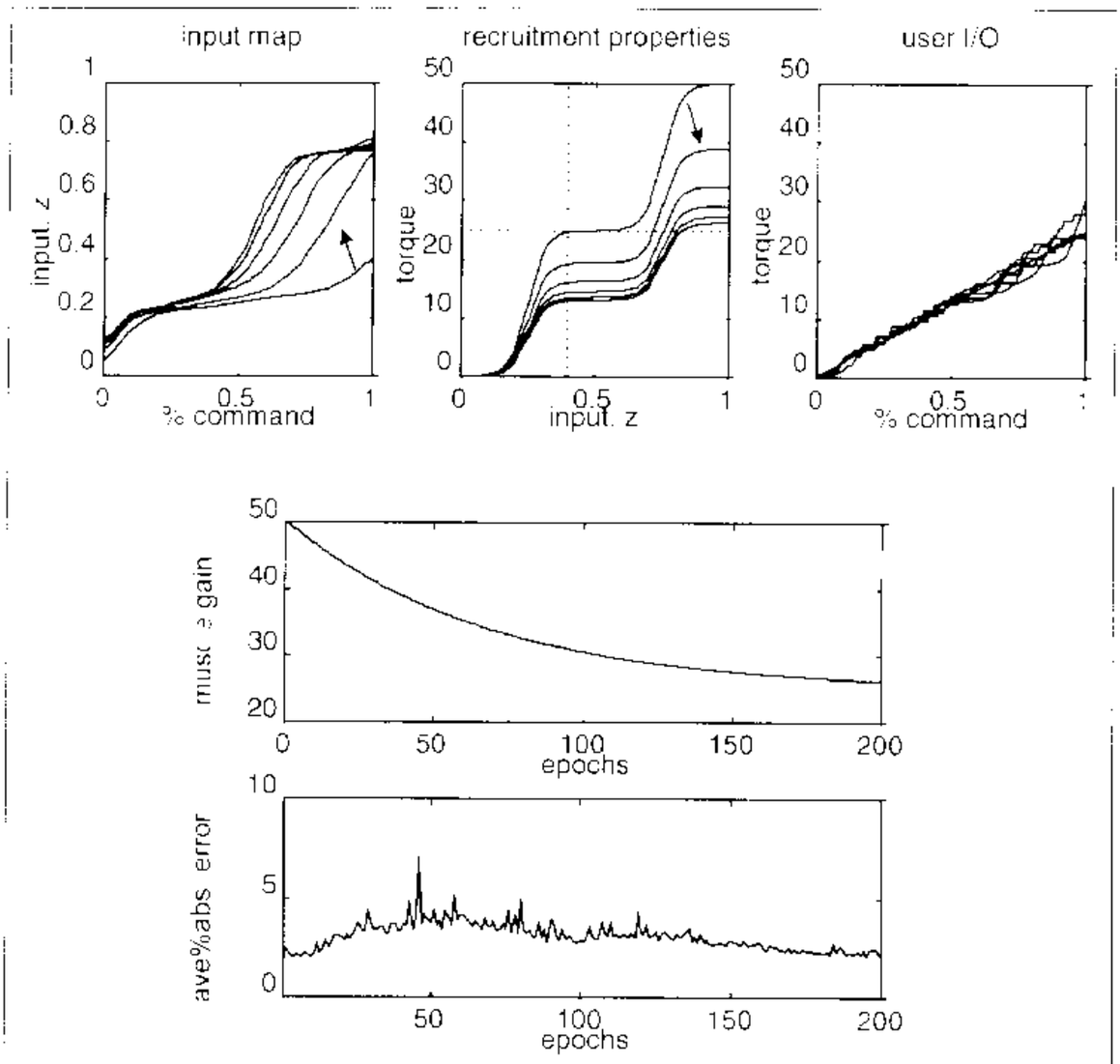

Figure 8: Simulation results demonstrating how the adaptive mapping scheme can maintain linear input/output properties as seen by the user as the muscle fatigues, even in the presence of complex nonlinearities in the recruitment properties. Descriptions of the plots are similar to those presented in Figure 7. In these simulations, recruitment curve model includes a 'double' nonlinearity in shape, and the model of muscle fatigue consists of a drop in muscle gain.

References:

1. Anthropology Research Staff (eds.). (1978). Anthropometric Source Book, Volume II: A Handbook of Anthropometric Data. (NASA Reference Publication 1024). Houston: NASA Scientific and Technical Information Office.
2. Gordon C.C., Churchill T., Clauser C.E., Bradtmiller B., McConville J.T., Tebbetts I., & Walker R.A. (1989). 1988 Anthropometric Survey of U.S. Army Personnel: Methods and Summary Statistics. Anthropology Research Project, Inc., US Army Development and Engineering Center, Natick.
3. Gilad I, Nissan M: A study of vertebra and disc geometric relations of the human cervical and lumbar spine. *Spine*, 11(2): 154-157, 1986.
4. Berry J, Moran JM, Berg WS, Steffee AD: A morphometric study of human lumbar and selected thoracic vertebrae. *Spine*, 12(4): 362-366, 1987.
5. Panjabi MM, Takata K, Goel V, Federico D, Oxland T, Duranceau J, Karg M: Thoracic human vertebrae: quantitative three-dimensional anatomy. *Spine*, 16(8): 888-901, 1991.
6. Scoles PV, Linton AE, Latimer B, Levy ME, Digiovanni BF: Vertebral body and posterior element morphology: the normal spine in middle life. *Spine*, 13(10): 1082-6, 1988.
7. Moga PJ, Erig M, Chaffin DB, Nussbaum MA: Torso muscle moment arms at intervertebral levels T10 Through L5 from CT scans on eleven male and eight female subjects. *Spine*, 18(15): 2305-2309, 1993.
8. Tracy M, Gibson MJ, Szypryt EP, Rutherford A, Corlett EN: The geometry of the muscles of the lumbar spine determined by magnetic resonance imaging. *Spine*, 14(2): 186-193, 1989.
9. Yamaguchi GT, Zajac FE: Restoring unassisted natural gait to paraplegics via functional neuromuscular stimulation: a computer study. *IEEE Trans Biomed Engr.*, 37(9): 886-902, 1990.
10. McConville JT, Churchill TD, Kaleps I, Clauser CE, Cuzzi J (1980). Anthropometric Relationships of Body and Body Segment Moments of Inertia. AFAMRL-TR-80-119, U.S. Air Force Aerospace Medical Research Laboratory, Wright Patterson Air Force Base, Ohio.